Structural Analysis and Response of Curved Prestressed Concrete Box Girder Bridges

DEEPAK CHOUDHURY AND ALEX C. SCORDELIS

A numerical procedure for linear-elastic analysis and nonlinear material analysis of curved prestressed concrete box girder bridges is demonstrated through two examples. A curved nonprismatic thin-walled box beam element is used to model the bridges. The cross section of the element is a rectangular single-cell box with side cantilevers. Eight displacement degrees of freedom, including transverse distortion and longitudinal warping of the cross section, are considered at each of the three element nodes. Prestressing, consisting of posttensioned bonded tendons in the longitudinal direction, is considered. For nonlinear material analysis, the uniaxial stress-strain curves of concrete, reinforcing steel, and prestressing steel are modeled. The shear and the transverse flexural responses of the box beam cross section are modeled using trilinear constitutive relationships based on cracking, yielding, and ultimate stages. The first example demonstrates the versatility of the numerical method in determining the linear-elastic distribution of forces in a three-span prestressed box girder bridge of curved plan geometry and variable cross section. Dead load, live load, and prestressing load cases are analyzed. In the second example, overload behavior and ultimate strength of a three-span curved prestressed concrete box girder bridge under increasing vehicular load are investigated. The different response characteristics of the bridge induced by different transverse locations of the overload vehicle are presented.

Prestressed concrete box girder bridges have gained importance as economic and esthetic solutions for the overpasses, underpasses, separation structures, and viaducts found in today's highway system. These bridges are often continuous-span structures (Figure 1a). Transverse diaphragms are placed at the end and interior support sections, and additional diaphragms are sometimes used between the supports. The typical cross section of such a box girder bridge consists of a top slab and a bottom slab connected monolithically by vertical webs to form a cellular or boxlike structure (Figure 1b). Design and esthetic considerations often call for longitudinal variations in the cross-sectional dimensions. In plan, the bridge can have a straight or curved geometry. Sometimes part of the bridge may be straight and part of it may be curved (Figure 1c). The complex spatial nature of a curved box girder bridge with a variable cross section (nonprismatic) makes it difficult to predict the structural response to a general loading case accurately. The presence of prestressing further complicates the analysis. Even with the assumption of homogeneous linear-elastic material, the accurate analysis of such a structure remains a formidable challenge to the engineer. Highway bridges are being subjected to increasing vehicular loads and traffic densities. A better understanding of the overload behavior of these bridges beyond the service load range is necessary. Also, in order to assess the degree of safety against failure, an accurate estimate of the ultimate load has to be made. A nonlinear analysis procedure incorporating the effects of nonhomogeneity of the material, concrete cracking, and nonlinearities in the stress-strain relationships of concrete reinforcing steel and prestressing steel is thus required. The objective of this paper is to demonstrate the capabilities of a numerical procedure for linear-elastic analysis and nonlinear material

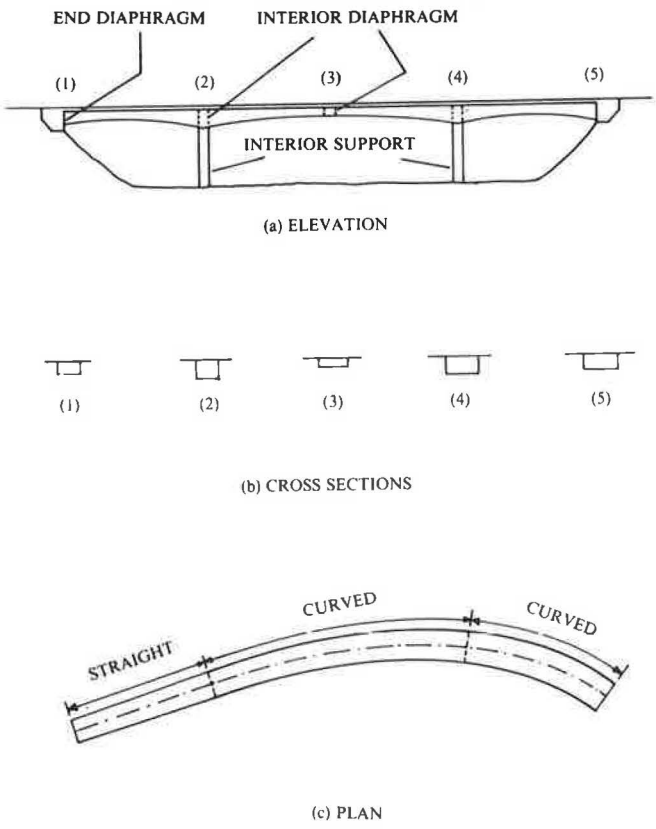

FIGURE 1 Curved nonprismatic box girder bridge.

D. Choudhury, T. Y. Lin International, 315 Bay Street, San Francisco, Calif. 94133. A. C. Scordelis, Department of Civil Engineering, University of California, Berkeley, Calif. 94720.

analysis of curved nonprismatic prestressed concrete box girder bridges. The overall response of the structure, rather than the local behavior, is studied.

METHOD OF ANALYSIS

The method of analysis employed in the present study uses a finite-element formulation based on thin-walled beam theory (*1, 2*). The theoretical details, summarized briefly in this paper, have been presented elsewhere (*3*).

Curved Nonprismatic Box Beam Element

Thin-walled box beam elements have been used by several investigators (*4–6*) for linear-elastic analysis of box girder bridges. These elements are capable of capturing the dominant structural actions, but at considerably reduced computational effort. The simplicity and reduced computational effort inherent in a beam-type element make it particularly suitable for nonlinear analysis, which requires much greater central processing unit time and storage space in the computer than linear-elastic analysis. Thus in the present study, certain aspects of the formulations used by Bazant and El Nimeiri (*4*) and by Zhang and Lyons (*5*) are combined to develop a curved nonprismatic thin-walled box beam element that can be easily extended to nonlinear analysis.

The three-node element is shown in Figure 2. Its axis lies in the global *X-Y* plane and may be curved. The cross section of the element perpendicular to its axis is a rectangular, single-cell, thin-walled box with side cantilevers. The dimensions of the box cross section, indicated in Figure 2b, can all vary along the length of the element. The geometry of the element is defined using an isoparametric mapping between the three nodes. The shape functions associated with the three nodes are second-order Lagrangian polynomials.

At each element node, eight generalized displacement degrees of freedom are considered. These are the usual six degrees of freedom associated with the rigid body translations and rotations of the cross section and, in addition, a longitudinal warping mode and a transverse distortional mode of the cross section (Figure 3). A generalized strain and its associated generalized stress are used to represent the strain energy contribution from transverse bending of the walls of the box cross section caused by the transverse distortional mode (Figure 3b). Also, the longitudinal normal strains and stresses and the shear strains and stresses acting in the plane of the cross section along the walls of the box are monitored.

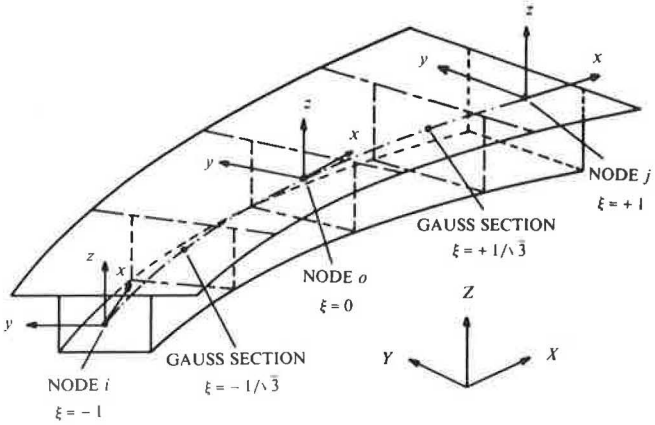

(a) ISOMETRIC VIEW

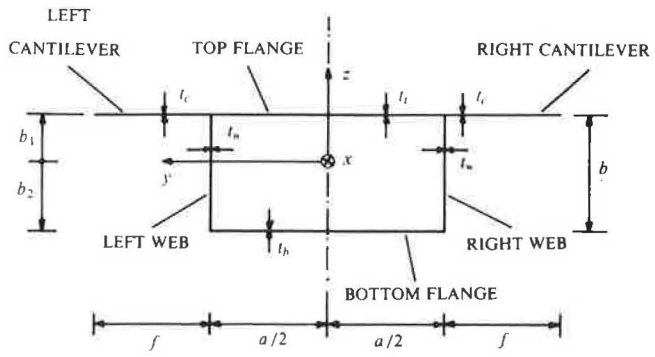

(b) CROSS SECTION

FIGURE 2 Curved nonprismatic thin-walled box beam element.

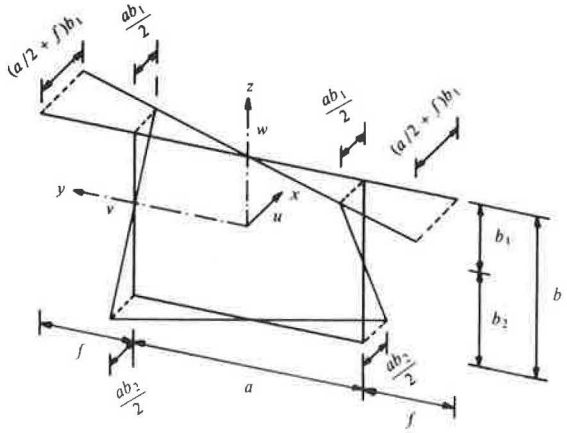

(a) UNIT LONGITUDINAL WARPING

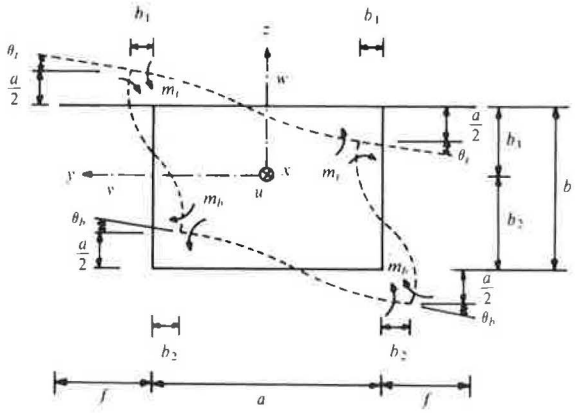

(b) UNIT TRANSVERSE DISTORTION

FIGURE 3 Longitudinal warping and transverse distortional modes.

The element property matrices are obtained numerically using two-point Gaussian quadrature along the element axis. This is found to eliminate the spurious shear stiffness usually associated with beam and shell formulations, including shear deformations. Spurious shear effects relative to the torsional, distortional, and warping degrees of freedom are also eliminated by this reduced order of integration.

Prestressing

Prestressing, by means of posttensioned tendons in the longitudinal direction, is considered. The tendons are idealized as straight prestressing steel segments between the nodes of the box beam elements. Friction and anchorage slip losses are considered. For linear-elastic analysis of the structure under prestressing, the effect of prestress is represented by a set of equivalent loads applied at the nodes of the box beam elements. For the analysis at transfer of prestress in a nonlinear analysis, the prestressing is similarly represented by a set of equivalent nodal loads, and the structure is analyzed as if it were of ordinary reinforced concrete. The contribution of the prestressing steel to the overall structural stiffness is neglected because at this stage the steel is unbonded. For the subsequent application of external loads, the prestressing steel is assumed to be bonded to the concrete (i.e., grouted), and the prestressing steel stiffnesses are included in the overall structural stiffness.

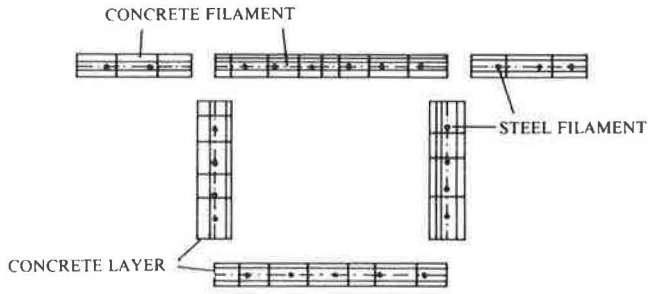

FIGURE 4 Box cross section discretized into concrete and longitudinal reinforcing steel filaments.

Nonlinear Analysis Procedure

For nonlinear material analysis, the box beam elements are considered to be concrete elements reinforced with steel in the longitudinal and transverse directions. In order to model the response of the reinforced concrete box beam element under longitudinal normal strains and stresses, the element cross section is idealized as concrete and longitudinal steel filaments that are assumed to be in a state of uniaxial stress (Figure 4). The uniaxial stress-strain curve adopted for the concrete filaments is based on the widely used relationship in compression suggested by Hognestad (7), together with cracking in tension at the tensile strength. With additional assumptions for load reversal, a total of 11 possible material states are obtained (Figure 5a). For the longitudinal steel filaments, a bilinear stress-strain relationship with load reversal is used (Figure 5b). Four different material states are possible. In addition, the tension-stiffening effect between the concrete and the steel filaments is modeled with a "steel-referred" method.

The trilinear constitutive relationship shown in Figure 5c is used to represent the shear response of the walls of the box section. The model incorporates the cracking, yielding, and ultimate stages. The postcracking behavior is based on the 45-degree truss analogy. The possibility of load reversal is considered, which gives a total of five different material states.

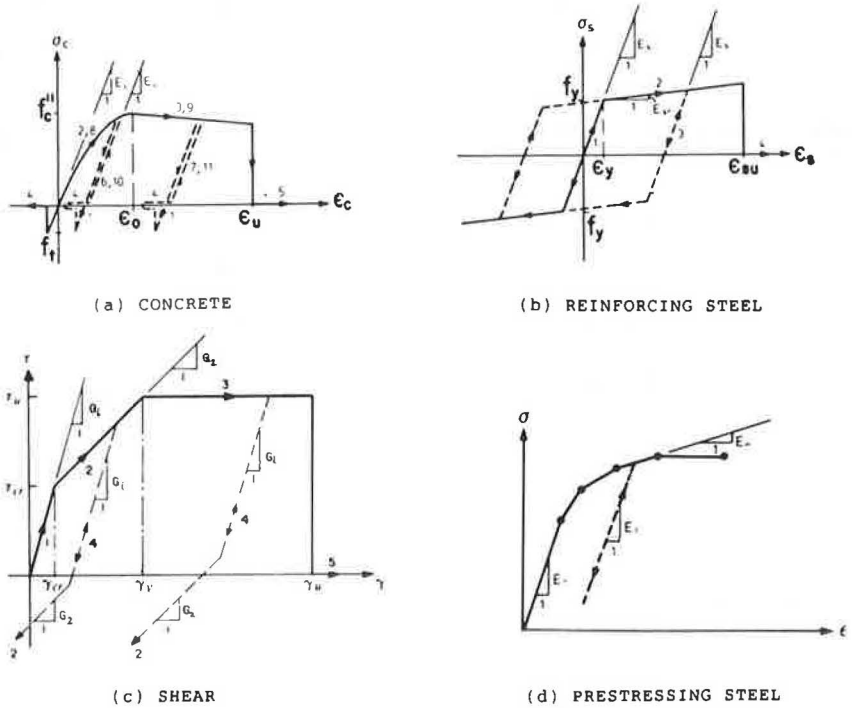

FIGURE 5 Nonlinear constitutive models.

The constitutive relationship for transverse flexure is obtained from a flexural analysis of the box beam cross section as a transverse reinforced concrete frame of unit width in the longitudinal direction. The resulting response is modeled with a trilinear relationship similar to the one used for shear (Figure 5c).

The uniaxial stress-strain relationship of the prestressing steel segments is modeled by using a multilinear idealization with load reversal (Figure 5d).

Because of the nonlinearities in the constitutive relationships, the equilibrium equations of the structure are nonlinear. These nonlinear equilibrium equations are solved in increments. Increments of either prescribed loads or displacements are applied, and for each increment unbalanced load iterations are performed until certain predefined convergence criteria are satisfied. With this nonlinear analysis procedure, the structural response can be traced throughout the elastic, inelastic, and ultimate load ranges.

COMPUTER PROGRAMS

The method of analysis has been incorporated into two computer programs: LAPBOX for linear-elastic analysis, and NAPBOX for nonlinear material analysis. The basic input for both programs consists of structure geometry and boundary conditions, material properties, prestressing data, structure loading, and locations for stress output. In addition, NAPBOX requires data on concrete and longitudinal steel filaments, transverse steel, and convergence tolerances. The various generation schemes implemented in the programs allow accurate modeling of complex bridge geometries, loadings, and prestressing tendon profiles on the basis of a few simple input parameters.

The computer programs LAPBOX and NAPBOX have been verified (*3*). Linear-elastic solutions from LAPBOX were compared with the folded-plate elasticity method (*8*), the finite-strip method (*9*), and the experimental results from a tapered box girder (*10*). NAPBOX results were compared with the computer program PCFRAME (*11*) for the special case of planar loading. PCFRAME, which is capable of performing nonlinear analysis of planar prestressed concrete frames, has been extensively tested (*11, 12*).

Detailed information on the theoretical basis, input and output, and a computer tape containing the source listings for LAPBOX and NAPBOX is available by writing to the second author.

EXAMPLE 1: LINEAR-ELASTIC ANALYSIS

Example 1 demonstrates the applicability of the proposed method and the capabilities of the computer program LAPBOX in determining the linear-elastic distribution of forces in a complex prestressed concrete box girder bridge of curved plan geometry and variable cross section.

Structure Details and Analytical Modeling

A hypothetical three-span continuous prestressed concrete box girder bridge (Figure 6) is analyzed. In plan (Figure 6a), the bridge has a straight span of 140 ft between supports S1 and S2, and two circularly curved spans of 240 ft between supports S2 and S3 and 180 ft between supports S3 and S4. The radius

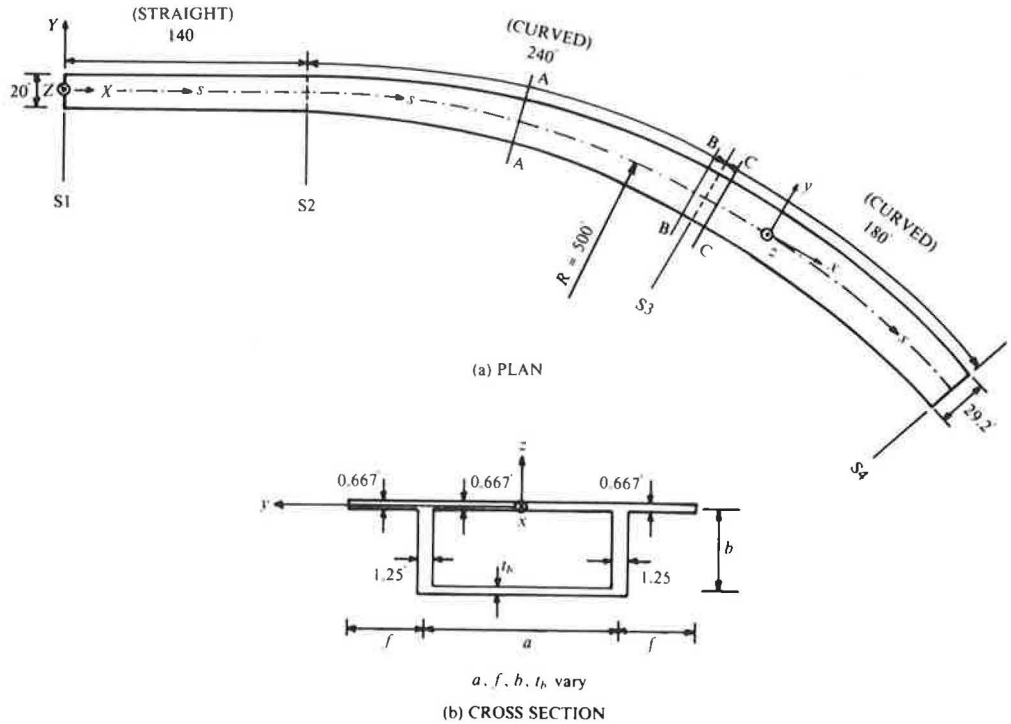

FIGURE 6 Example 1: three-span curved nonprismatic prestressed concrete bridge. (a) Plan view, (b) cross section.

of the circularly curved spans is R = 500 ft to the centerline. For convenience, a coordinate s is defined along the centerline with its origin at S1 and directed toward S4. At each of the four supports of the bridge, vertical movement, twist, and transverse distortion of the cross section are prevented.

The cross section of the bridge is shown in Figure 6b. The following equations define the variation of the cross-sectional dimensions a, f, b, and t_b (all in feet) in terms of the s-coordinate. A modulus of elasticity of 608,256 kips/ft^2 and a Poisson's ratio of 0.18 are assumed for the concrete.

a	$= 12 + s/100$	for $0 < s < 560$ ft
f	$= 4 + 9s/2800$	for $0 < s < 560$ ft
b	$= 6 + s/70$	for $0 < s < 140$ ft
	$= 52/3 - s/15$,	for 140 ft $< s <$ 200 ft
	$= 4$	for 200 ft $< s <$ 320 ft
	$= -52/3 + s/15$,	for 320 ft $< s <$ 380 ft
	$= 110/9 - s/90$	for 380 ft $< s <$ 560 ft
t_b	$= 3/5 + s/200$	for $0 < s <$ 140 ft
	$= 67/30 - s/150$	for 140 ft $< s <$ 260 ft
	$= -37/30 + s/150$	for 260 ft $< s <$ 380 ft
	$= 25/9 - 7s/1800$	for 380 ft $< s <$ 560 ft

The bridge is prestressed with 14 different tendons, 7 in each web (Figure 7). The jacking forces and the geometry data of each tendon are given in Table 1. Each tendon numbered 1 through 6 has a vertical profile along its span consisting of one parabolic segment. Each of the other 8 tendons has two parabolic segments connected by a linear segment in the middle. All the tendons are stressed simultaneously from both ends. A wobble friction coefficient of 0.0002/ft, a curvature friction coefficient of 0.2/radian, and no anchorage slip are assumed.

Three different load cases are considered. They may be summarized as follows:

Case 1: Dead load due to a unit weight density of 160 pcf.
Case 2: Prestressing.
Case 3: Uniform live load of 0.15 kip/ft^2 over the full width of the the top deck and between s = 180 ft and 340 ft.

TABLE 1 EXAMPLE 1: PRESTRESSING TENDON DATA

TENDON NO.	JACKING FORCE (kip)	LOCATION OF END A		LOCATION OF END B		LOCATION(S) OF ZERO TENDON SLOPE	
		s (ft)	z (ft)	s (ft)	z (ft)	s (ft)	z (ft)
1, 2	300	0	-2.470	120	-4.044	60	-6.357
3, 4	700	420	-3.646	560	-2.410	490	-6.278
5, 6	600	180	-2.473	340	-2.463	260	-3.500
7, 8	2500	80	-3.343	200	-1.710	120; 160	-0.500
9, 10	3000	320	-1.840	440	-3.283	360; 400	-0.500
11, 12	1000	40	-2.911	240	-1.710	80; 200	-0.500
13, 14	1250	280	-1.710	480	-4.089	320; 440	-0.500

The bridge is analyzed by using 56 curved nonprismatic box beam elements, each 10 ft long. All load cases are represented by equivalent nodal loads generated automatically within the program LAPBOX.

An additional analysis is performed for load case 3 with the computer program SAP IV (*13*) using 56 one-dimensional (straight) beam elements, each spanning 10 ft (measured along the actual axis of the bridge). Each element is prismatic, so the nonprismatic bridge can only be modeled approximately by using different cross-sectional properties for each element.

Results

Table 2 gives a summary of the support reactions obtained from LAPBOX for all load cases. In the last two columns, the total of all the vertical reactions is compared with the total applied load calculated by hand from the actual geometry and loading of the structure. The agreement is perfect, which is indicative of the high accuracy with which the box beam elements can be used to model the geometry and loading of a curved nonprismatic bridge. The support reactions obtained from the SAP IV analysis for load case 3 are also shown in Table 2. The agreement between the LAPBOX and the SAP IV results is good, particularly for the vertical reactions.

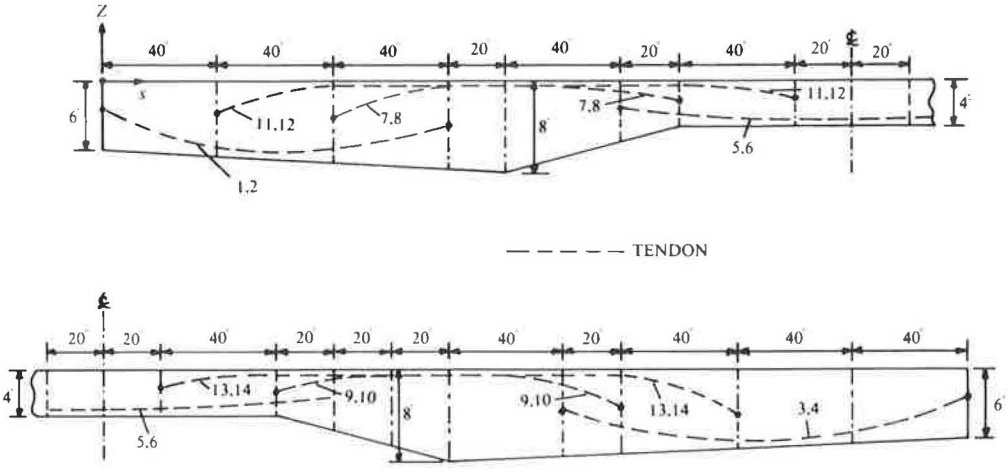

FIGURE 7 Example 1: three-span curved nonprismatic prestressed concrete bridge—longitudinal section along centerline.

TABLE 2 EXAMPLE 1: SUMMARY OF SUPPORT REACTIONS

LOAD CASE	FORCE QUANTITY	SUPPORT S1	SUPPORT S2	SUPPORT S3	SUPPORT S4	TOTAL VERTICAL REACTION (kip)	TOTAL APPLIED LOAD (kip)
DEAD LOAD	Distortional Moment M_d (kip·ft)	-0.2	782.4	2233.6	-125.1	—	—
	Vertical Force V_z (kip)	237.8	1491.9	1853.2	493.8	4076.7	4076.7
	Torque M_x (kip·ft)	-2.8	-867.9	-2026.8	1545.0	—	—
PRE-STRESS	Distortional Moment M_d (kip·ft)	-0.1	260.1	572.3	14.6	—	—
	Vertical Force V_z (kip)	-30.8	26.4	34.2	-29.8	0.0	0.0
	Torque M_x (kip·ft)	-1.6	-1103.6	-1954.8	-267.3	—	—
LIVE LOAD (LAPBOX)	Distortional Moment M_d (kip·ft)	-0.1	430.3	1035.3	8.0	—	—
	Vertical Force V_z (kip)	-116.2	404.0	385.2	-90.5	582.5	582.5
	Torque M_x (kip·ft)	-1.6	-322.9	-2359.2	-860.3	—	—
LIVE LOAD (SAP IV)	Vertical Force M_z (kip)	-115.7	403.4	385.2	-90.4	582.5	582.5
	Torque M_x (kip·ft)	0	-344.2	-2384.0	-848.0	—	—

The longitudinal variations of the vertical centerline displacements are shown in Figure 8. The plotted values for the live load case represent both the LAPBOX and the SAP IV analyses, which predicted practically the same vertical displacements. The transverse distributions of the vertical displacements at the middle of the interior span (s = 260 ft) are shown in Figure 9. The vertical displacements are larger at the outer web than at the inner web, with almost a linear variation across the bridge width, which indicates a twist of the cross section with little transverse distortion.

Longitudinal variations of bending moments for dead load, prestressing, and live load are shown in Figures 10 through 12,

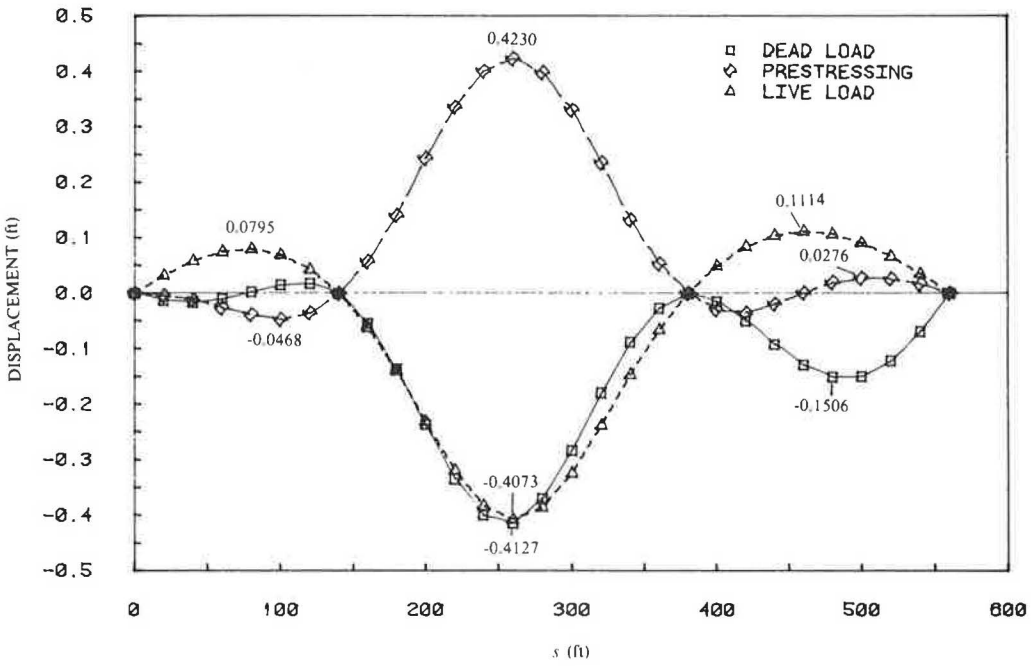

FIGURE 8 Example 1: longitudinal distributions of vertical centerline displacements.

respectively. It should be noted that the moments are with respect to the local y-axes of the cross sections (Figure 6b). When axial loads are present, which is the case with prestressing, the plotted moments will differ from the moments about the neutral axes of the cross sections. The locations of the discontinuities in the prestressing moment diagram (Figure 11) correspond to the tendon ends. The live load moments (Figure 12) obtained from the LAPBOX and the SAP IV analyses are found to agree closely.

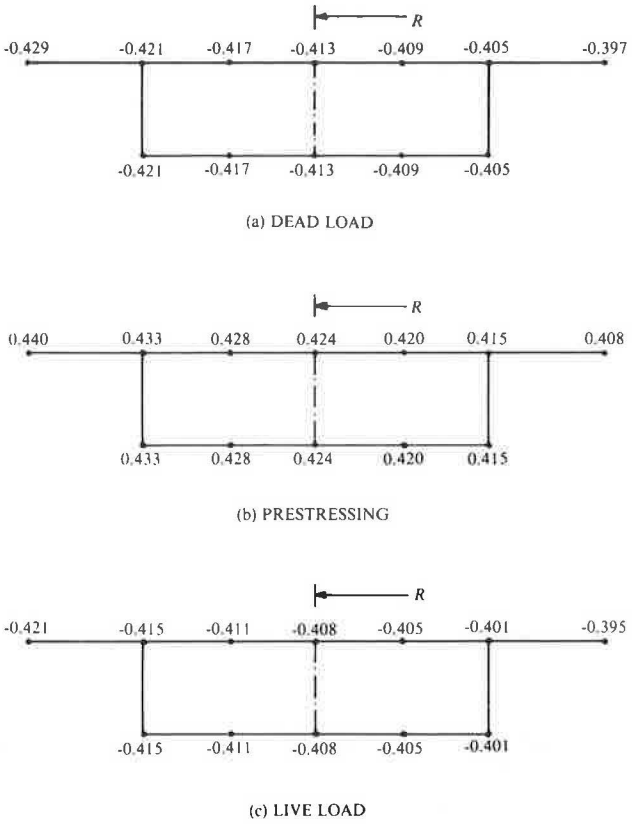

FIGURE 9 Example 1: transverse distributions of vertical displacements (s = 260 ft).

The close agreement between the LAPBOX and the SAP IV results for the live load case indicates that the longitudinal flexural behavior of the bridge was not affected significantly by transverse distortion and longitudinal warping of the cross sections. However, ordinary beam theory (SAP IV) cannot predict the transverse distribution of stresses and the transverse flexural moments (not reported), which can be obtained from thin-walled beam theory (LAPBOX).

EXAMPLE 2: NONLINEAR ANALYSIS

Example 2 demonstrates how the proposed nonlinear analysis procedure can be used to trace the response of a curved prestressed concrete box girder bridge throughout the elastic, inelastic, and ultimate load ranges. Overload behavior and ultimate strength of the bridge under increasing vehicular load are investigated. The different response characteristics of the bridge, induced by different transverse locations of the overload vehicle, are presented.

Structure Details and Analytical Modeling

The three-span, curved, continuous, prestressed concrete box girder bridge considered in this example is shown in Figure 13. Its span arrangement is symmetric, with spans of 160, 200, and 160 ft. The axis of the bridge is circularly curved in plan with a radius of R = 496.5 ft to the centerline. Full restraint against vertical translation, twist, and transverse distortion of the cross section at the four supports is assumed.

For the sake of simplicity, the cross section (Figure 13b) is assumed to be constant from one end of the structure to the

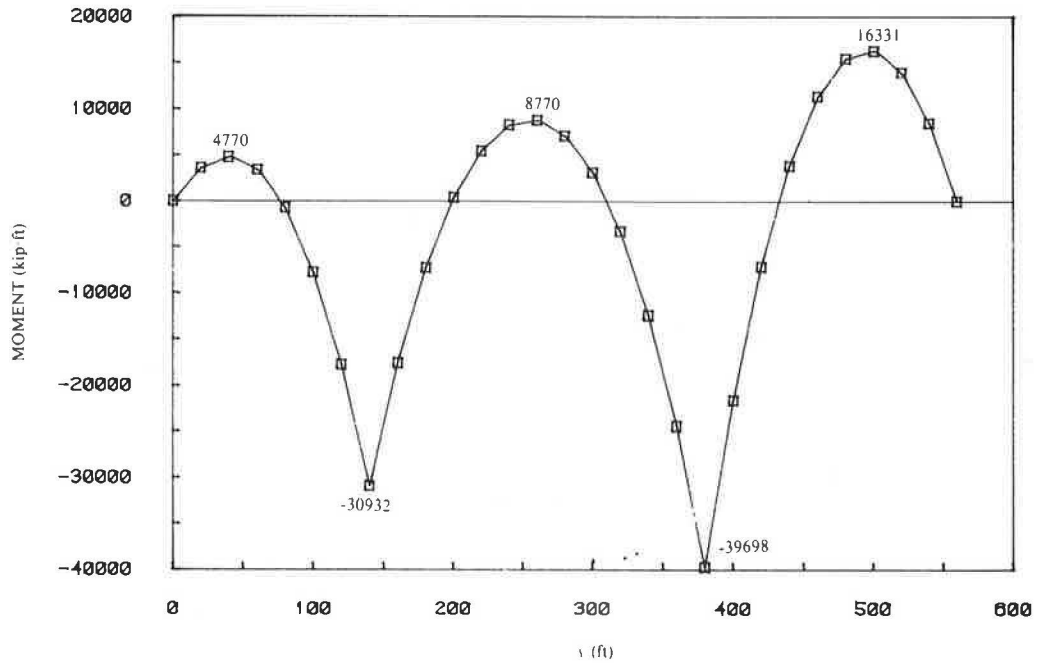

FIGURE 10 Example 1: longitudinal distribution of bending moment M_y due to dead load.

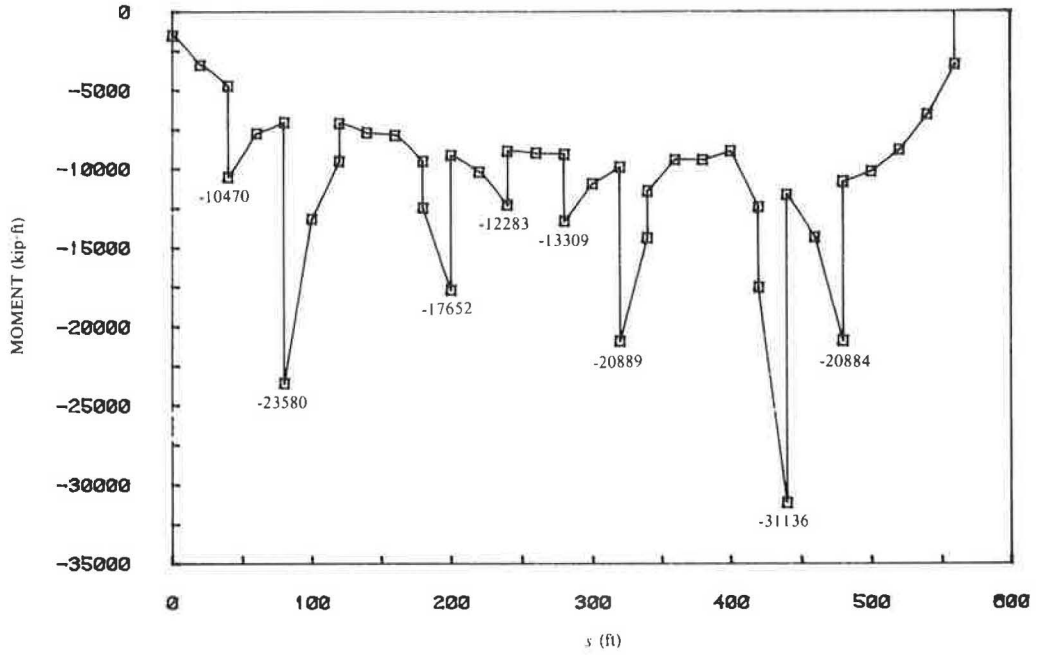

FIGURE 11 Example 1: longitudinal distribution of bending moment M_y due to prestressing.

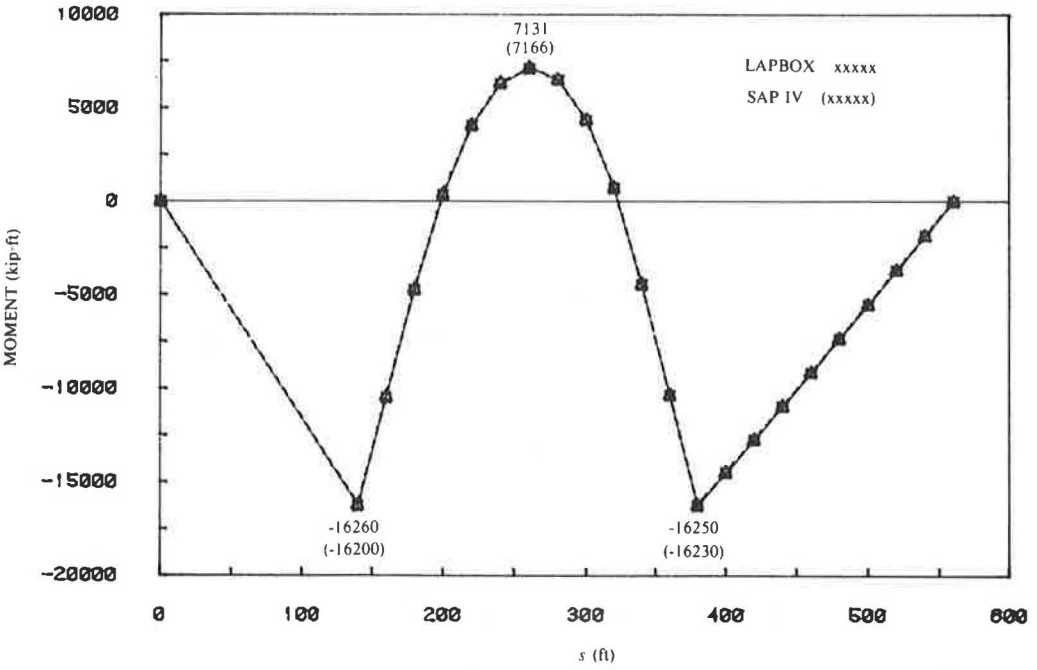

FIGURE 12 Example 1: longitudinal distribution of bending moment M_y due to live load.

ouer, although design considerations often call for thickening of the bottom flange or the webs, or both, in regions near the supports. The total top deck width of 34 ft is typical of a two-lane highway bridge.

The prestressing in the bridge consists of two tendons in the longitudinal direction, one in each web. The prestress is achieved by posttensioning from both ends simultaneously, after which the prestressing steel is grouted and hence bonded to the concrete. The tendon profile along the curved webs is the same in each web, and is shown in Figure 13c.

The following conditions are assumed: concrete compressive strength of 4,000 psi, mild steel yield strength of 60 ksi, prestressing steel ultimate strength of 270 ksi, wobble friction coefficient of 0.0002/ft, curvature friction coefficient of 0.25/radian, anchorage slip at each jacking end of 0.25 in., and unit weight of composite structure of 155 pcf.

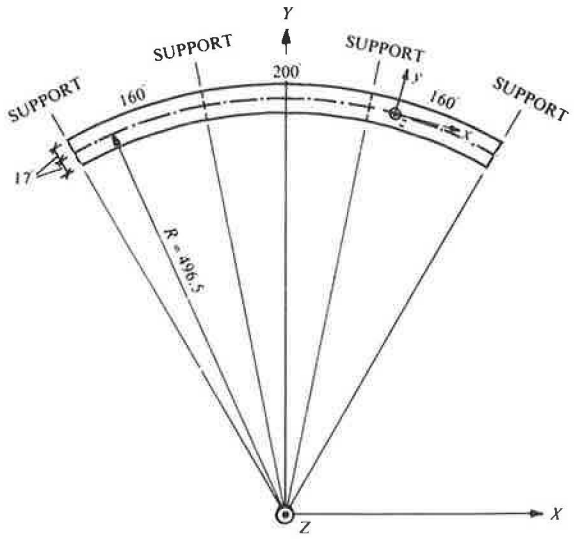

(a) PLAN

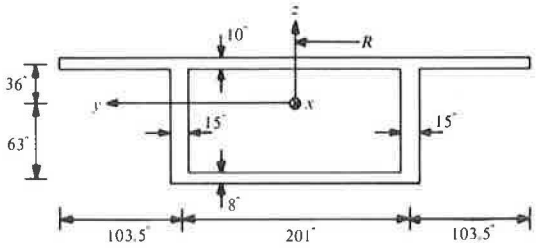

(b) CROSS SECTION

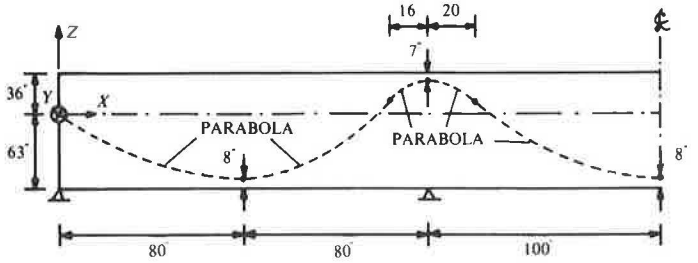

(c) PRESTRESSING TENDON PROFILE

FIGURE 13 Example 2: three-span curved prestressed concrete bridge.

Structural design of the box girder is based on State of California standard criteria (*14*). The prestressing steel requirements are calculated by considering HS20 lane loading in each of the two lanes, impact factors on the basis of span lengths, and an allowable tensile stress of 6 $(f_c')^{1/2}$ psi in concrete after all prestressing losses have occurred. A total of 172 seven-wire strands with 0.5-in. diameter (86 strands per web), which gives a total prestressing steel area of 26.32 in.^{2}, is provided. The required jacking force is 2,660 kips per web. Ultimate strength under factored loads is checked. In the load factor design, an additional overload vehicle, designated a P13 truck (Figure 14), is considered.

Longitudinal mild steel reinforcement corresponding to 0.3 percent of the concrete area is provided in each wall of the box cross section. This steel is not required because of strength considerations, but is provided for construction purposes. The transverse reinforcement consists of two legs of No. 5 stirrups at 4-in. longitudinal spacing in each web and two legs of No. 5 stirrups at 10-in. longitudinal spacing in each slab.

The response of the bridge structure is studied under increasing levels of vehicular overload. The overload vehicle, the P13 truck (Figure 14), is typical of the heaviest vehicles found on California's highways. In order to take advantage of the symmetry of the structure, the P13 truck loading in Figure 14b is approximated with the symmetric loading in Figure 14d. This symmetric truck loading is positioned in the middle of the center span of the bridge (Figure 15a), and the structural load vector due to its weight is increased in increments until ultimate failure occurs. For convenience in presentation of results, P is used to denote the factor of truck load applied. Thus $P = 1$ represents the overload due to one truck (Figure 15a).

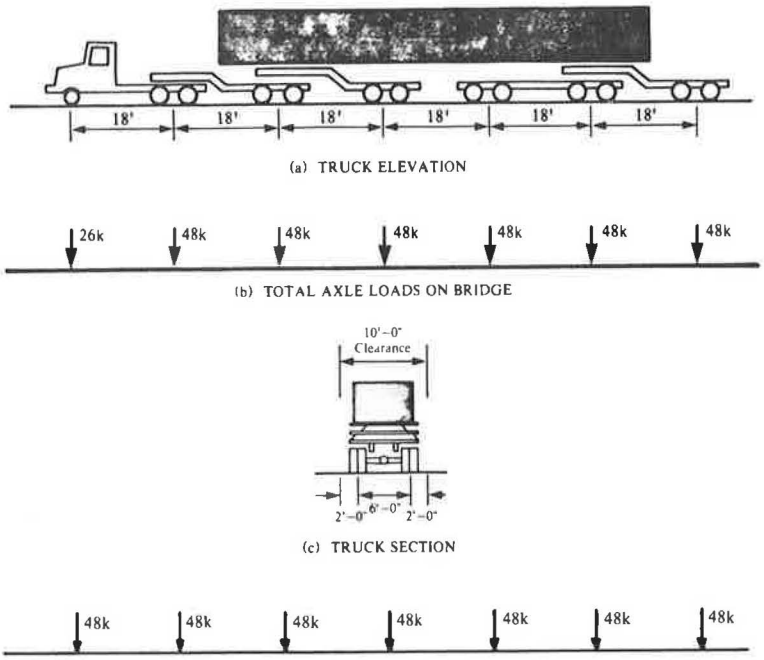

FIGURE 14 Example 2: P13 truck loading.

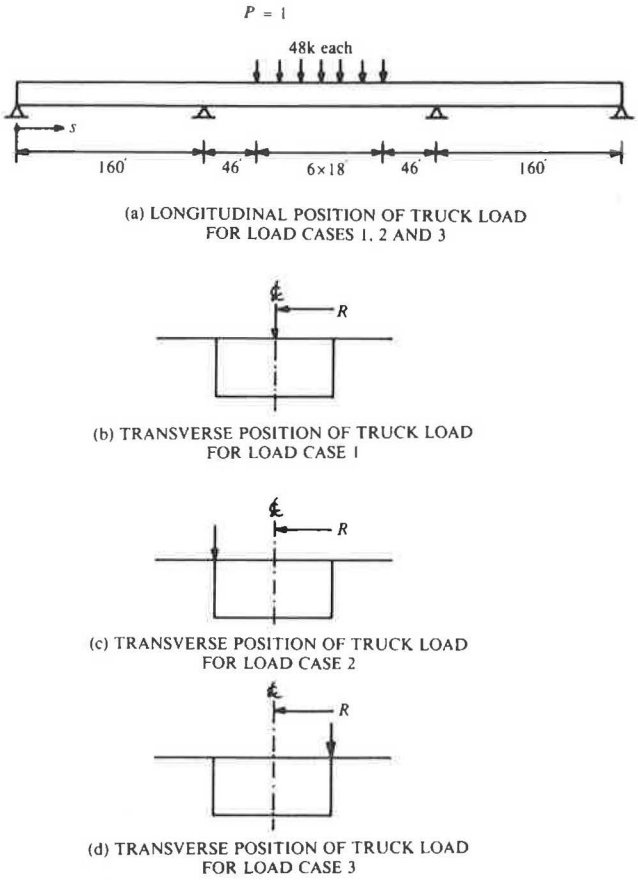

FIGURE 15 Example 2: position of truck load for different load cases.

Three different load cases are considered:

Case 1: Truck load positioned over bridge centerline (Figure 15b).

Case 2: Truck load positioned over outer web (Figure 15c).

Case 3: Truck load positioned over inner web (Figure 15d).

Because of the symmetry of the structure and the loadings, only half the length of the bridge is analyzed. Forty curved box beam elements of varying lengths are used. The cross section is discretized into 52 concrete and 26 longitudinal steel filaments.

Results

Figures 16 through 18 show the vertical web displacements at the middle of the center span under increasing truck loads for load cases 1, 2, and 3, respectively. It is evident from the load-displacement curves that the structure responds quite differently depending on the transverse position of the truck load.

Load case 1 (Figure 16), with the truck load over the centerline, yielded the highest ultimate load of $P = 5.6$. Failure occurred because of the yielding of concrete filaments in compression at the bottom flange over the interior supports. The small differences between the vertical displacements at the two webs indicate that the overall response of the bridge was governed by its longitudinal flexural behavior.

In Figure 17, the differences between the vertical displacements at the two webs are seen to be quite significant for load case 2, in which the truck load is positioned over the outer

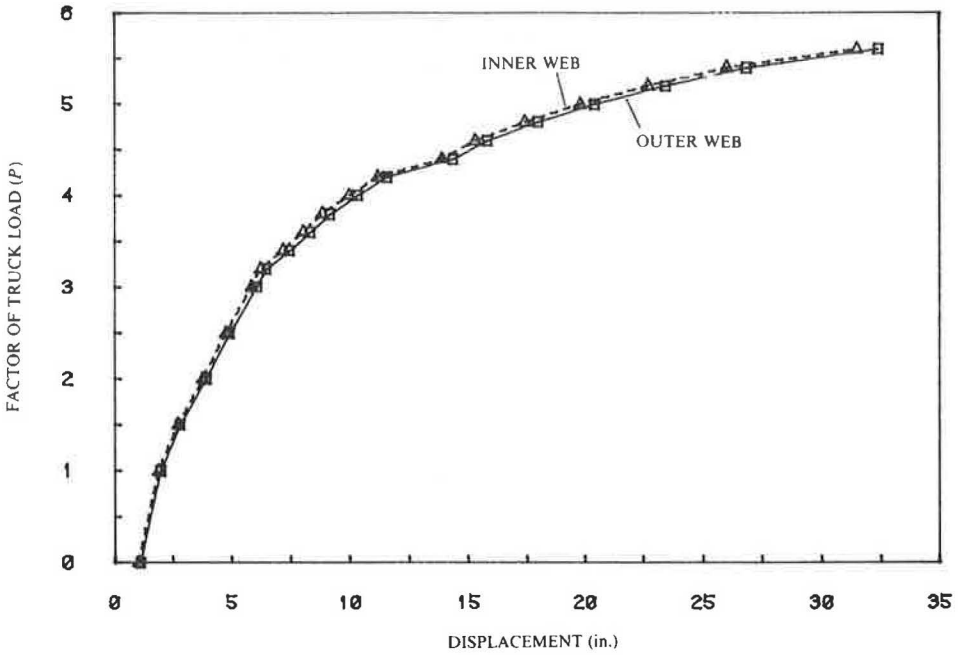

FIGURE 16 Example 2: load versus vertical web displacements at middle of center span (load case 1).

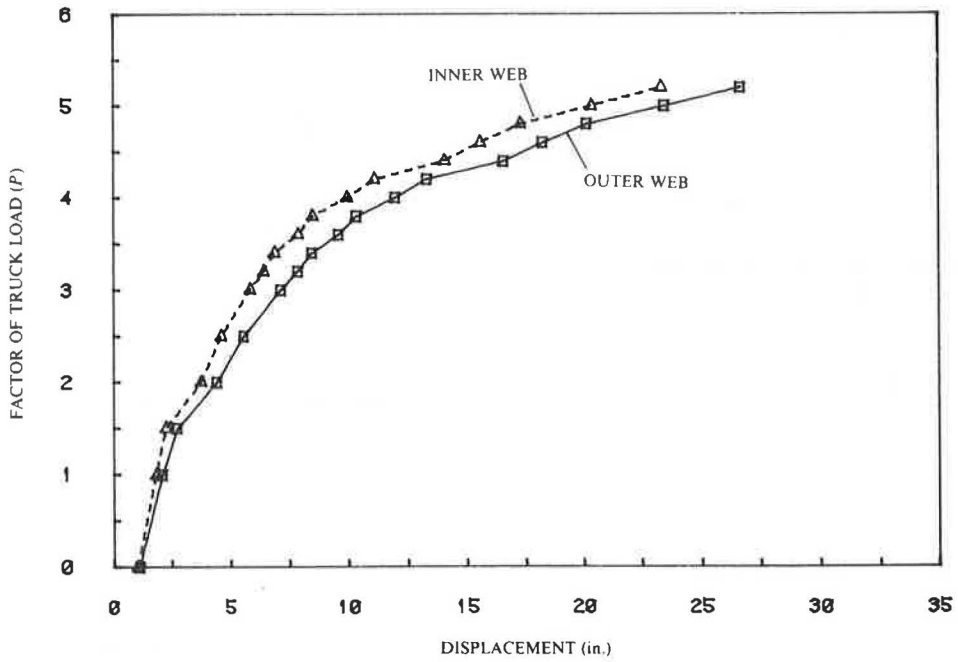

FIGURE 17 Example 2: load versus vertical web displacements at middle of center span (load case 2).

web. The differential web displacements, which increase with increasing load levels, are primarily due to the twist of the cross section and were caused by rapid deterioration in the torsional stiffness of the bridge. The ultimate load of the bridge was reduced to $P = 5.2$. Failure occurred when the shear stress reached its ultimate value at the outer web of the sections just to the inside of the interior supports.

An ultimate load of only $P = 4.0$ was obtained for load case 3 (Figure 18), with the truck load positioned over the inner web. This loading produced rapid deterioration in the

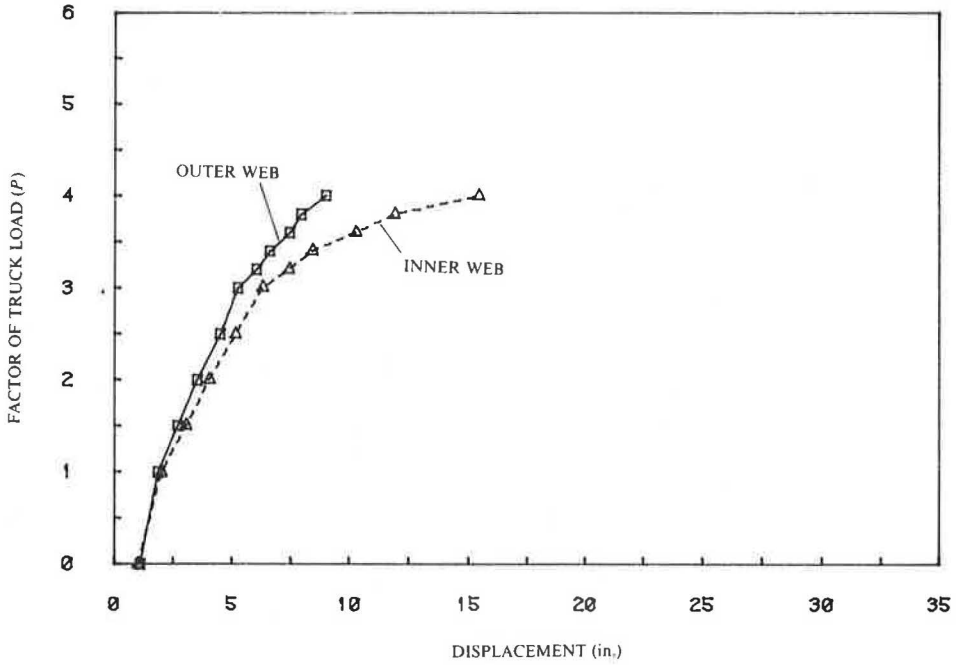

FIGURE 18 Example 2: load versus vertical web displacements at middle of center span (load case 3).

transverse flexural rigidity of the bridge. The transverse distortion of the cross section at the middle of the center span increased rapidly, and this is reflected in the increasingly large differences between the vertical displacements at the two webs. Failure was due to the ultimate transverse distortion of the cross section at the middle of the center span, which is governed by the plastic hinge rotation capacities at the four corners of the box section.

The cross-section twists at the middle of the center span are shown in Figure 19 for all three load cases. The rapid deterioration in the torsional stiffness of the bridge for load case 2 is evident. Of the three load cases considered, load case 2 represents the most severe torsional loading. The outer web loading tends to twist the cross section in the same direction as the dead load and prestressing, and hence produces the largest cross-section twists. Load case 1 produces a less severe

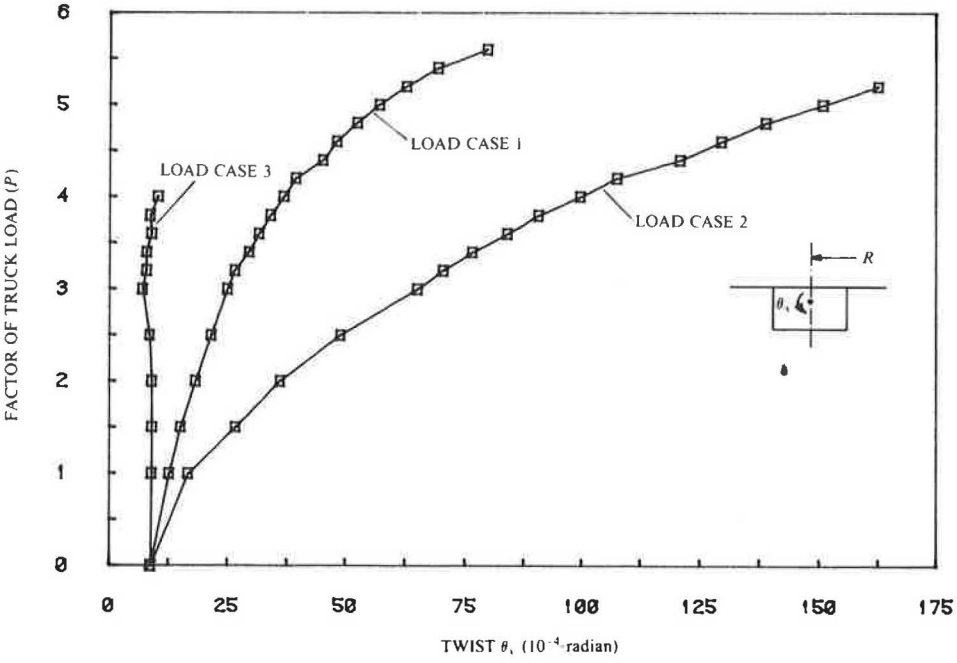

FIGURE 19 Example 2: load versus cross-section twist at middle of center span (load cases 1–3).

torsional response of the bridge. Because of the curvature of the bridge axis, the centerline loading does tend to twist the cross section, but its effect is not as pronounced as that of load case 2. Load case 3 represents the least severe torsional loading. The inner web loading tends to decrease the cross-section twist due to dead load and prestressing. The net result is that the cross-section twist remains almost constant with increasing truck load levels.

The transverse distortions of the cross section at the middle of the center span are shown in Figure 20 for the three load cases. Load case 3 is now found to produce the most severe response. The inner web loading tends to distort the cross section in the same direction as the dead load and prestressing. The combined effect is to cause rapid deterioration in the transverse flexural rigidity of the cross section. Initial cracking due to transverse flexure was observed at the middle of the center span at the very first load step of $P = 1.0$. This was followed by transverse flexural yielding at the same location at $P = 2.5$. Beyond $P = 2.5$, the transverse distortions increased rapidly as the transverse flexural yielding spread longitudinally. At the ultimate load of $P = 4.0$, the yielding spread to about 82.5 ft from the middle of the center span. The transverse distortions for load cases 1 and 2 are seen in Figure 20 to be much smaller than those for load case 3. No serious deterioration in the transverse flexural rigidity was observed for either of these load cases.

The prestressing steel segment stresses at two critical locations, one near the middle of the center span and the other near the interior support, are shown in Figure 21 for load cases 1 and 2 and in Figure 22 for load case 3. For each location, the prestressing stresses in both webs are shown. The differences between the initial stresses in the two webs are very small because the higher wobble friction losses in the outer web more or less balance out the higher curvature friction losses in the inner web.

The load levels at which initial cracking of concrete filaments was observed at the middle of the center span and at the interior support are summarized in Table 3. These cracking loads can be identified in Figures 21 and 22 as the points at which large increases in the tendon stresses occur.

The differences between the tendon stresses in the two webs, evident in Figures 21 and 22, provide further insight into the behavior of the bridge under the three different loading conditions. A higher tendon stress in one or the other web indicates that a greater proportion of the load is carried by that web. Figure 21a shows that for load case 1, a greater proportion of the load is carried by the inner web near the middle of the center span. Near the interior support, the outer web carries a greater proportion of the load. However, the small differences between the tendon stresses in the two webs at both locations also indicate that the centerline truck loading is distributed fairly uniformly across the width of the bridge. In Figure 21b, practically equal proportions of the outer web loading are found to be carried by the two webs near the middle of the center span. Near the interior support, the outer web carries a considerably greater proportion of the load. Figure 22 shows that for load case 3, increasingly greater proportions of the inner web loading are carried by the inner web with increasing load levels. At both critical locations, the differences between the tendon stresses in the two webs increase rapidly after the initiation of concrete filament cracking. Near the middle of the center span, the outer web tendon stresses in fact start to decrease near the ultimate, whereas the inner web tendon stresses continue to increase rapidly. The increasing deterioration in the ability of the box section to distribute the eccentrically applied inner web loading transversely is due

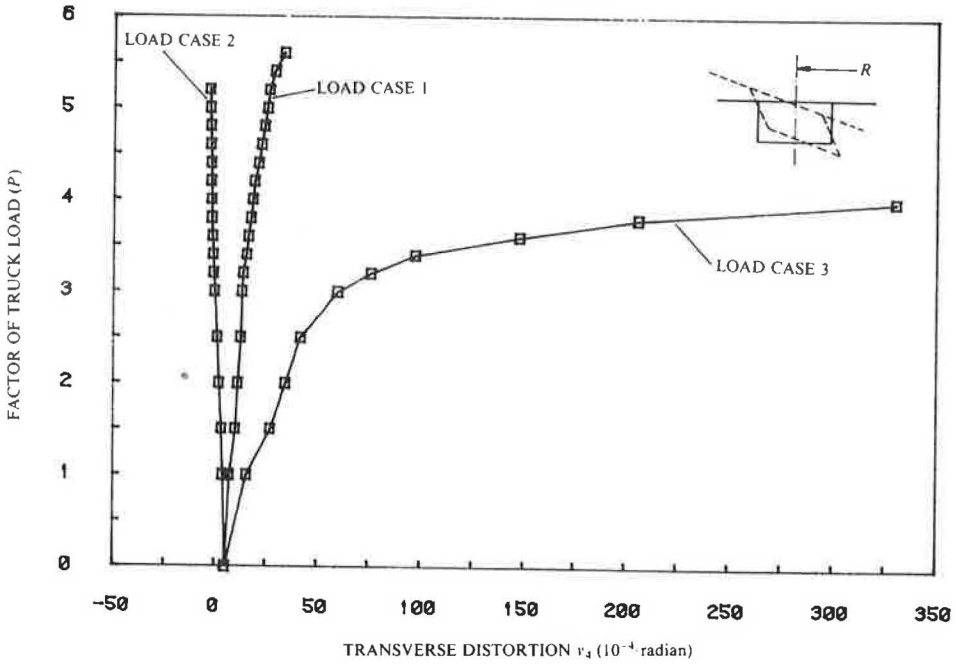

FIGURE 20 Example 2: load versus transverse distortion of cross section at middle of center span (load cases 1–3).

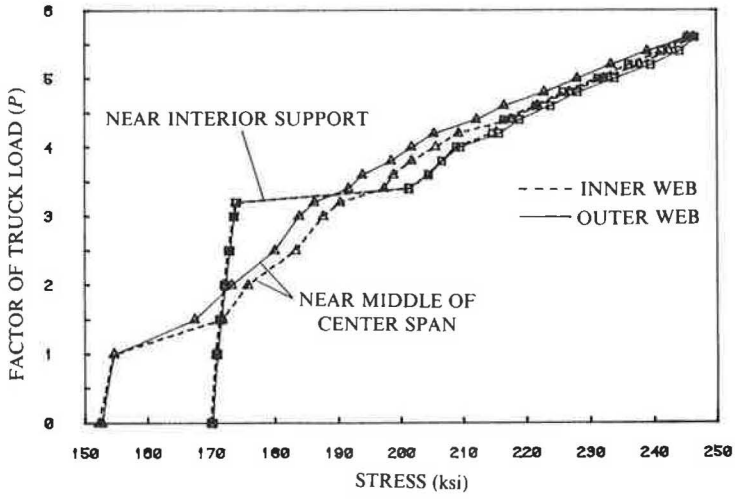

(a) LOAD CASE 1

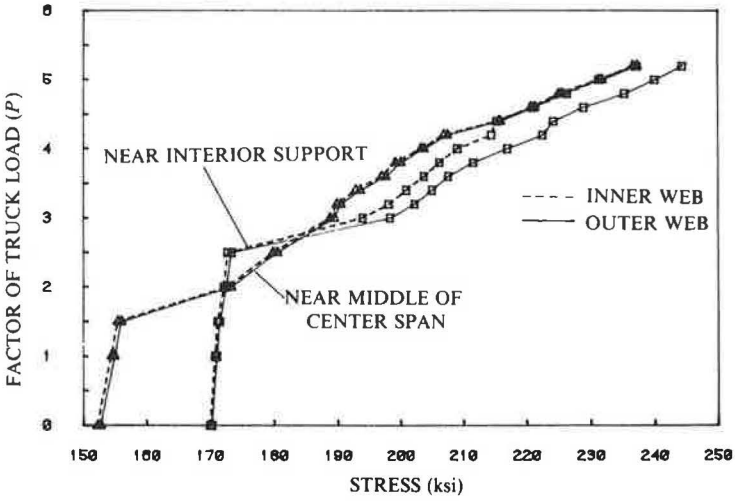

(b) LOAD CASE 2

FIGURE 21 Example 2: load versus prestressing steel segment stresses at critical locations (load cases 1 and 2).

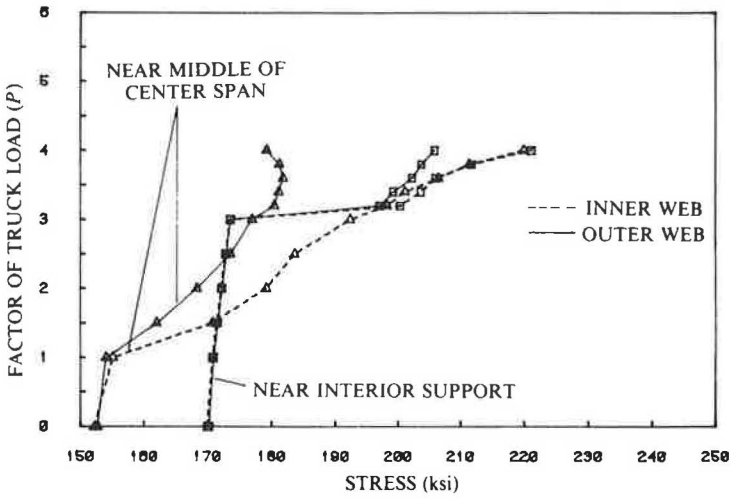

FIGURE 22 Example 2: load versus prestressing steel segment stresses at critical locations (load case 3).

TABLE 3 SUMMARY OF CRACKING LOADS

LOAD CASE	INITIAL CRACKING AT MIDDLE OF CENTER SPAN	INITIAL CRACKING AT INTERIOR SUPPORT
CENTERLINE LOAD	P = 1.5	P = 3.4
OUTER WEB LOAD	P = 2.0	P = 3.0
INNER WEB LOAD	P = 1.5	P = 3.2

to the rapid deterioration in the transverse flexural rigidity of the bridge.

CONCLUSIONS

The capabilities and usefulness of the proposed analytical method for curved prestressed concrete box girder bridges have been amply demonstrated. The nonlinear analysis procedure is shown to be capable of capturing the dominant structural behavior in the elastic, inelastic, and ultimate load ranges. Internal strains and stresses in concrete, reinforcing steel, and prestressing steel can be determined at all loading stages. Useful information on overload behavior and ultimate strength can be obtained from such a detailed analysis. Depending on the structure and the loading, warping, distortional, and torsional effects can influence structural behavior significantly. They not only affect the internal force distribution within the box structure, but also may govern the failure mode and the ultimate load.

ACKNOWLEDGMENT

This research was performed at the University of California, Berkeley, under the sponsorship of the U.S.-Spain Joint Committee for Scientific and Technological Cooperation.

REFERENCES

1. V. Z. Vlasov. *Thin-Walled Elastic Beams.* Israel Program for Scientific Translations, Jerusalem, Israel, 1961.
2. R. Dabrowski. *Curved Thin-Walled Girders: Theory and Analysis.* Springer-Verlag, New York, 1968.
3. D. Choudhury. *Analysis of Curved Nonprismatic Reinforced and Prestressed Concrete Box Girder Bridges.* Structural Engineering, Mechanics and Materials Report UCB/SEMM-86/13. University of California, Berkeley, Dec. 1986.
4. Z. P. Bazant and M. El Nimeiri. Stiffness Method for Curved Box Girders at Initial Stress. *Journal of the Structural Division,* ASCE, Vol. 100, No. ST10, Oct. 1974, pp. 2071–2090.
5. S. H. Zhang and L. P. R. Lyons. A Thin-Walled Box Beam Finite Element for Curved Bridge Analysis. *Computers and Structures,* Vol. 18, No. 6, 1984, pp. 1035–1046.
6. M. J. Mikkola and J. Paavola. Finite Element Analysis of Box Girders. *Journal of the Structural Division,* ASCE, Vol. 106, No. ST6, June 1980, pp. 1343–1357.
7. E. Hognestad. *A Study of Combined Bending and Axial Load in Reinforced Concrete Members.* Bulletin Series 399, Bulletin 1. University of Illinois Engineering Experiment Station, Urbana-Champaign, Nov. 1951.
8. A. DeFries-Skene and A.C. Scordelis. Direct Stiffness Solution for Folded Plates. *Journal of the Structural Division,* ASCE, Vol. 90, No. ST3, June 1964, pp. 15–47.
9. Y.K. Cheung. Finite Strip Method Analysis of Elastic Slabs. *Journal of the Engineering Mechanics Division,* ASCE, Vol. 94, No. EM6, Dec. 1968, pp. 1365–1378.
10. V. Kristek. Tapered Box Girders of Deformable Cross Section. *Journal of the Structural Division,* ASCE, Vol. 96, No. ST8, Aug. 1970, pp. 1761–1793.
11. Y. J. Kang and A. C. Scordelis. Nonlinear Analysis of Prestressed Concrete Frames. *Journal of the Structural Division,* ASCE, Vol. 106, No. ST2, Feb. 1980, pp. 445–472.
12. J. Hellesland, D. Choudhury, and A. C. Scordelis. *Nonlinear Analysis and Design of RC Bridge Columns Subjected to Imposed Deformations.* Structural Engineering and Structural Mechanics Report UCB/SESM-85/03. University of California, Berkeley, April 1985.
13. K. Bathe, E. L. Wilson, and F. E. Peterson. *SAP IV: A Structural Analysis Program for Static and Dynamic Response of Linear Systems.* Earthquake Engineering Research Center Report EERC 73-11. University of California, Berkeley, June 1973.
14. *Standard Specifications for Highway Bridges.* American Association of State Highway and Transportation Officials, Washington, D.C., 1983, 13th edition. Revised by California Department of Transportation.

Publication of this paper sponsored by Committee on Concrete Bridges.